Ketogenic diet as a metabolic vehicle for enhancing the therapeutic efficacy of mebendazole and devimistat in preclinical pediatric glioma

Purna Mukherjee[1], Bennett Greenwood[2], Juan Henao[2], Michael A. Kiebish[2], and Thomas N. Seyfried[1]

1- Department of Biology, Boston College, Chestnut Hill, MA 02467
2- BPGbio Framingham, MA 01701

Corresponding author: Thomas N. Seyfried, PhD. Email : thomas.seyfried@bc.edu

Abstract

Invasion of high-grade glioma (HGG) cells through the brain and spinal cord is a leading cause of cancer death in children. Despite advances in treatment, survivors often suffer from life-long adverse effects of the toxic therapies. This study investigated the influence of nutritional ketosis on the therapeutic action of mebendazole (MBZ) and devimistat (CPI-613) against the highly invasive VM-M3 glioblastoma cells in juvenile syngeneic p20-p25 mice; a preclinical model of pediatric HGG. Cerebral implantation of the VM-M3 glioblastoma cells invaded throughout the brain and the spinal column similar to that seen commonly in children with malignant glioma. The maximum therapeutic benefit of MBZ and CPI-613 on tumour invasion and mouse survival occurred only when the drugs were administered together with a ketogenic diet (KD). MBZ reduced VM-M3 tumour cell growth and invasion when evaluated under *in-vitro* and *in-vivo* conditions through inhibition of both the glutaminolysis and the glycolysis pathways. Moreover, administration of the drugs with the KD allowed a low dosing for the juvenile mice, which minimized toxicity while improving overall survival. This preclinical study in juvenile mice highlights the potential importance of a diet/drug therapeutic strategy for managing childhood brain cancer.

Introduction

The alarming rise in incidence of glioblastoma (GBM) across all age groups over the last 21 years requires immediate action for management and prevention (1-3). Diffusely infiltrating pediatric high-grade gliomas (HGGs) are the leading cause of cancer death in children in the US with no improvement in management in over 10 years (4-7). Most survivors experience multiple adverse effects that significantly reduce quality of life (8). HGGs have been classified as anaplastic astrocytoma, diffuse intrinsic pontine glioma (DIPG), and glioblastoma multiforme (GBM) (9). Interestingly, glioma cell dissemination through cerebrospinal fluid (CSF) is more common in pediatric HGG patients than in adult glioma patients with similar histopathology. CSF involvement could explain the poor survival prognosis in pediatric HGG patients (6, 10).

The incidence of metastatic spread has been reported as 2–14 % of adult glioma patients at the time of tumor recurrence (10, 11). The pattern of recurrence of pediatric malignant gliomas can be different from that reported for adults, given the significant incidence of distant relapse and high risk of leptomeningeal dissemination (12). Although the role of macrophage/microglia in invasion and metastasis is debatable, substantial evidence shows that cells expressing microglia/macrophage markers comprise 30–50% of the cells in malignant gliomas including the tissue of DIPG and GBM (13-15). We previously proposed that some of the microglia/macrophages present in the glioma tissue are part of the neoplastic malignant cells themselves and, given their mesenchymal amoeboid properties, maybe capable of invading the surrounding parenchyma giving rise to tumor growth and even tumor metastasis (16). In that respect, our clonal population of VM-M3 cells, which arose spontaneously in the brains of VM/Dk mice, are highly aggressive and metastatic regardless of whether the cells are implanted orthotopically or subcutaneously in the mice (17, 18). The rapid growth and distal brain invasion of the VM-M3 tumor cells through Scherer's structures is also remarkably similar to those features seen in human glioblastoma (18). In this study the spinal invasion of VM-M3 cells from the cerebral cortex in postnatal mice shows similar etiology to that of pediatric HGG.

The response to chemotherapy is poor in most pediatric brain cancer patients with survivors experiencing unacceptable toxicity and reduced quality of life (19, 20). Temozolomide chemotherapy, which has only modest therapeutic benefit in adult glioma patients, is overly toxic and without therapeutic benefit for pediatric brain cancer patients (21). This failure is likely due to the metabolic properties of the neoplastic tumor cells. In contrast to the complex genetic heterogeneity seen in gliomas, aerobic glucose fermentation (Warburg effect) is the common metabolic phenotype seen in most high-grade pediatric and adult gliomas (HGG) (22-24). In addition to aerobic carbohydrate fermentation, brain tumor cells are also dependent on glutamine fermentation for growth and survival (24-26). The reliance on glucose and glutamine for glioma malignancy comes from the well-documented defects found in mitochondrial OxPhos (27). Glucose and glutamine fermentation in the cytoplasm and mitochondria, respectively, can compensate for OxPhos impairment. We recently showed how the glutamine antagonist, 6-diazo-5-oxo-L-norleucine (DON), administered together with a calorically restricted ketogenic diet (KD-R) managed late-stage orthotopic growth in two syngeneic mouse models of GBM (28). DON targets glutaminolysis, while the KD-R reduces glucose and, simultaneously, elevates ketone bodies that are neuroprotective and non-fermentable. The diet/drug therapeutic strategy killed tumour cells while reversing disease symptoms and improving overall survival. Moreover, the KD-R diet facilitated DON delivery to the brain and allowed a lower dosage to achieve therapeutic effect**.** As drug delivery to the pediatric brain is considered a major limitation to effective management of HGG, mechanisms underlying brain drug delivery will have immediate and significant impact for children with brain cancer.

The antiparasitic drug, mebendazole (MBZ), showed preclinical efficacy in models of GBM and medulloblastoma (29, 30). A phase I clinical trial for newly diagnosed HGG pediatric patients has been initiated for MBZ (ClinicalTrials.gov Identifier: NCT01837862). This trial will evaluate safety and dosing in treating pediatric patients with recurrent or refractory gliomas. MBZ treatment *in-vivo* as a single agent or in combination with chemotherapy led to the reduction or complete arrest of tumor growth, marked decrease in metastatic spread, and increase in overall survival (31-33). The mechanism by which MBZ inhibits tumor growth is due in part to the inhibition of glucose uptake and glycolytic enzymes (34, 35). MBZ has relatively low toxicity in both adults and in children (36-38). As systemic bioavailability is best when MBZ is administered

orally with fatty foods (39, 40), we administered MBZ with a ketogenic diet to young mice with invasive VM-M3 glioma in this study.

The lipoate derivative CPI-613 is a novel anti-cancer agent that targets mitochondrial dehydrogenase activities (pyruvate dehydrogenase and α-ketoglutarate dehydrogenase) causing apoptosis, necrosis, and autophagy of tumor cells (41-45). CPI-613 had little toxicity in therapeutic dose ranges and was well-tolerated at higher doses in preclinical models (the maximum tolerated dose in mice was 100 mg/kg). CPI-613 (10 mg/kg) significantly inhibited the growth of the H460 human non-small cell lung carcinoma in xenograft mice. CPI-613 also caused robust tumor growth inhibition in a mouse model of human pancreatic tumor (BxPC-3)(46). Although CPI-613 was therapeutic against preclinical cancers, it failed to show non-toxic therapeutic efficacy against metastatic pancreatic cancer and relapsed or refractory acute myeloid leukemia in two phase III clinical trials (47-49). There are currently no clinical or preclinical reports on the use of CPI-613 for managing brain tumors.

Here we show for the first time that devimistat (CPI-613) and MBZ are therapeutically synergistic when administered together with a ketogenic diet in juvenile mice with invasive VM-M3 brain tumor. Moreover, we report for first time that MBZ can target the glutaminolysis pathway of VM-M3 cells both *in-vitro* and *in-vivo*. These findings further support the dependency of the invasive VM-M3 glioma cells on glutamine for growth. Both drugs prevented dissemination of the VM-M3 tumor cells from the brain to the spinal cord when administered together with the KD in young mice. Moreover, minimal drug dosages could achieve remarkable non-toxic improvement in overall survival when administered with the KD. This novel diet/drug cocktail therapy will have significant translational impact for children with malignant brain cancers.

Results

The aim of this research was to determine if a ketogenic diet could improve the therapeutic action of MBZ and CPI-613 against the progression of the VM-M3 preclinical glioblastoma in the juvenile mouse brain (p20-p25). The mouse brain at these ages is comparable to that of children between 3-7 years of age (50). None of the mice received radiation or steroids as a part of the metabolic treatment protocol in order to avoid the provocative effects of elevated blood glucose and systemic inflammation on tumor growth (51, 52). Survival of the mice was measured as a secondary end point. DON treatment alone was used as a positive control throughout the study based on our previous observations (28). The juvenile mice were fed *ad libitum* to maintain body weight.

VM-M3 glioblastoma cells invade the spinal cord from the brain implantation site in young mice.

VM-M3 tumour cells (100,000 cells in 5.0 ul PBS) were implanted into the brains of young postnatal-day p20-25 mice of the syngeneic VM/Dk inbred strain. The mice were imaged for bioluminescence on day 6 after tumour implantation to ensure tumor take. It is interesting to note that the VM-M3 tumour cells invaded the spinal cord from the brain implantation site (**Figure 1A & 1B**). We have not previously seen spinal cord invasion of VM-M3 tumour cells when implanted into the brains of adult VM/Dk mice (28). Furthermore, spinal cord invasion was not seen following brain implantation of the non-invasive VM-NM glioma stem cell tumour into young mice (**Figure 1C**). It is also important to mention that cerebrospinal dissemination of malignant glioma is more commonly seen in children than in adults and is indicative of very poor survival. Hence, our pre-clinical model is highly relevant to the situation seen in children with malignant glioma.

KD enhances the therapeutic effects of MBZ and DON against VM-M3 glioblastoma cell growth in brain and spread to spinal cord in young mice.

After bioluminescence imaging, the mice were divided into diet/drug groups. MBZ was administered to the mice in the KD (100 mg/kg body weight) for 3 consecutive days/wk. The KD, without MBZ, was administered alone on the off days. The study was terminated when the mice in the chow-fed control group lost about 20% body weight and developed signs of morbidity. All mice were imaged to evaluate brain tumour growth *in-vivo* before removing the brains for *ex-vivo* imaging. DON (1.0 mg/kg body weight) was injected intraperitoneal (i.p.) once or twice/wk. Each experiment was repeated 3-4 times in the same way when mouse litters became available. Male and female mice from each litter were randomly distributed among the groups, i.e., both males and females were tested for each drug.

The following experiments were used to evaluate the effect of MBZ and DON on the growth and invasion of VM-M3. **Experiment 1**, was a preliminary study on a single litter of 5 young mice that included a mouse chow diet control, a ketogenic diet (KD) control, a KD + MBZ experimental, and a KD + DON experimental. This study involved both *in-vivo* and *ex-vivo* imaging of brains. **Experiment 2** involved the repeat of Experiment 1 in another set of young mice from the same litter. This study involved *ex-vivo* imaging. **Experiment 3** included only two groups; a mouse chow diet control group and a KD + MBZ experimental group. **Experiment 4** involved the combinatorial effects of MBZ and DON on the survival of the young mice. We chose not to evaluate the efficacy of these drugs administered in the high-carbohydrate chow diet based on previous studies showing that therapeutic efficacy of MBZ and DON is best when the drugs are administered in high-fat diets (28, 30),

Experiment 1, the imaging data in **Figure 1D-G** show that brain bioluminescence, indicated as number of photons x 10^x, was significantly lower, both *in-vivo* and *ex-vivo,* in the mice treated with KD + MBZ or with KD + DON than in either mouse group receiving the KD alone or in the two mice that received the chow diet alone. The photon measurement is indicative of tumour ATP synthesis and viability. The greater the bioluminescence (photon counts) the faster the tumour growth while the lower the bioluminescence the slower the tumour growth (17).

We found that the diet/drug cocktails prevented tumour cell spread through the CSF. **(Figure 1F).** Also, bioluminescence was greater on the "right" ipsilateral side (tumour implanted side) than on the left contralateral side of the brains. Bioluminescence detected on the "left" contralateral side

is indicative of distal tumour cell hemispheric invasion. No bioluminescent tumour cells were detected on the "left" contralateral brain side of the mouse treated with KD + DON indicating that this treatment significantly reduced both growth and distal invasion of the VM-M3 tumour cells. **Figure 1G** shows the quantitation of photon values in different groups. **Experiment 2**, showed that brain bioluminescence was highest in mice that received the mouse chow diet (Chow Control). Although brain bioluminescence was lower in the mice that received the KD alone (KD Control) than in the mice that received Chow alone, the greatest reductions in brain bioluminescence were seen in the KD + MBZ and KD + DON groups indicating a significant diet/drug therapeutic synergy **Figure 1H**. **Experiment 3,** involved a further evaluation of KD + MBZ compared to chow control group. *Ex-vivo* bioluminescent photon values were compared for individual p20 mice that were either untreated (Chow control) or treated with KD + MBZ (100 mg/kg body**).** Brain photons were counted 12 days after brain implantation of VM-M3 tumour cells. It is clear that VM-M3 tumour cell bioluminescence was significantly lower in the mice receiving KD + MBZ than in the mice receiving the control chow diet (**Figure 1I)**. The photon values from the pooled data of all the mice in the in KD + MBZ group were significantly lower than those from the two controls groups **Figure 1J**. These findings show that administration of MBZ or DON with KD caused a significant reduction in tumor growth. The data from **Experiment 4** showed that overall survival was longer in the KD-fed mice than in the chow fed control mice, but that the overall survival was significantly longer in mice receiving the KD containing either MBZ or DON than in mice receiving the KD alone (**Figure 1K)**. The mice on diet/drug therapy were ambulatory and appeared healthy in contrast to the control chow-fed mice that were sedentary and appeared moribund (Supplementary video). Histopathological analysis revealed massive tumour cell death without obvious invasion in the brains of a mouse fed the KD + MBZ diet (**Figure 1L)**.

MBZ targets both the glutaminolysis and the glycolysis pathways in cultured VM-M3 cells

VM-M3 cells were treated *in-vitro* with different doses of MBZ and DON. DON was used as a positive control for these experiments as our previous studies showed that DON targets the glutaminolysis pathway by inhibiting multiple glutaminases (53, 54). Media and cells were collected at different times for LC-MS analysis of metabolites and bioluminescence for cell viability. VM-M3 cells (1×10^5) were seeded in 24-well plates using DMEM and 10% FBS. After 24 hours, the cells were rinsed with PBS and then grown in serum free basal media with 12.0 mM

glucose and 2.0 mM glutamine. The cells were cultured for another 24 hrs. in MBZ (vehicle DMSO) or DON using different drug doses.

MBZ treatment reduced the bioluminescence in the VM-M3 cells in a dose dependent manner (**Figures 2A**). Brightfield images showed that MBZ killed the VM-M3 cells at the highest dose **Figure 2E**). DON reduced the proliferation rate of VM-M3 cells (**Figure 2B, F**), but did not kill the cells as we reported previously (54). In contrast to MBZ, which showed a dosage effect for viability, no dosage effect for proliferation was seen for DON. Based on this information, we used 1.0 uM of MBZ and 50 uM of DON in further experiments. About 50% of the tumour cells were killed after 24 hours of the treatment (**Figure 2C**). To study the effect of MBZ on the glycolysis and the glutaminolysis pathways of VM-M3 cells, we altered the glucose and the glutamine levels in serum free basal media. VM-M3 cells (1×10^5) were seeded in 24 wells as before. After 24 hors., the cells were rinsed with PBS and treated with MBZ (1.0 uM) and DON (50.0 uM) in basal media for another 24 hours. **Figure 2G** shows that both glutamine and glucose are required for VM-M3 proliferation. MBZ treatment significantly reduced the proliferation as we noticed in **Figure 2C**. Interestingly, the inhibitory effect of MBZ was evident when glutamine was the only substrate present in the media, but was not seen when glucose was the only substrate. In the positive control study, DON-treated cells showed a similar result. These findings indicate that glutamine is more important than glucose for VM-M3 tumour cell viability suggesting that MBZ might influence viability through an effect on the glutaminolysis pathway. In the next experiment, VM-M3 cells were seeded in 6 wells plate. After 24 hrs. the cells were treated with MBZ (1.0 uM) for 2 hr., 6 hr., and 12 hr. in basal media with no FBS. The LC-MS metabolite data showed that the glutamine level was higher and the glutamate was lower in MBZ-treated cells than in the control cells after 2.0 hours (**Figures 2H-I**). These findings suggest that glutamine usage is important for the growth VM-M3 tumor cells. Restricted glutamine usage could also account in part for the lower levels seen for succinate, which is the end product of the glutaminolysis pathway (25, 27). MBZ apparently caused a reduction in glutaminolysis metabolites. This reduction could reduce ATP synthesis through mitochondrial substrate level phosphorylation at the succinyl CoA ligase step in the TCA cycle (25, 27, 55). This reduction could then reduce metabolite levels in the glycolytic pathway, as reflected at 6 hrs. **(Figures 2H-J).** Glutaminase C expression was significantly lower in the MBZ treated brain than in the control brain (**Figure 2K).** DON was used

as a positive control. These results suggest that MBZ targets both the glutaminolysis and the glycolysis pathways in the VM-M3 tumor cells.

CPI-613 reduces the growth of VM-M3 cells *in-vitro* and *in-vivo*

VM-M3 cells were treated with different doses of CPI-613 as described above in **Figure 2** for the MBZ experiment. CPI-613 reduced the bioluminescence of the VM-M3 tumour cells in a dose dependent manner (**Figure 3A**). Moreover, CPI-613 (100 uM) killed approximately 50% of the VM-M3 tumour cells after 24 hours of the treatment. VM-M3 tumour cells (100,000 cells in 5 ul) were implanted into the brains of young postnatal-day 20-25 mice of the inbred VM/Dk strain as described above. The mice were imaged on day 6 after tumour implantation. After bioluminescence imaging, the mice were divided into four diet/drug groups that included: A chow diet control; a Chow diet + CPI 613; a Ketogenic diet (KD) control, and a KD + CPI 613 (0.5-1.0 mg/kg body weight in DMSO) injected intraperitoneal (i.p.) once/wk.

Both the chow control diet and the control KD mice received only the DMSO vehicle. The mice were imaged *in-vivo* on day 13 after tumour implantation. Bioluminescence was high in mice fed the chow and in mice fed the chow + CPI-613 indicating that CPI-613 was largely ineffective by itself in lowering VM-M3 cell growth. On termination, *ex-vivo* bioluminescence measurements were lower in the mice fed KD + CPI than in the other groups suggesting a synergistic therapeutic effect of CPI-613 with the KD (**Figure 3B**). These findings are important, as no prior studies have evaluated the therapeutic action of CPI-613 against brain cancer when administered with the KD.

CPI-613 enhances the survival of young mice with orthotopic CT-2A tumor.

In addition to evaluating the therapeutic effects of CPI-613 on the orthotopic growth of the VM-M3 glioblastoma cells in their syngeneic VM/Dk host strain at postnatal-day 20-25, we also evaluated the therapeutic effects of CPI-613 on the orthotopic growth of the CT-2A stem cell glioma in the syngeneic C57BL/6J host strain at postnatal-day 20-25. Overall mouse survival was significantly longer when CPI-613 was used together with the KD than when used with chow diet. DON was used as a glutamine-targeting positive control for these experiments (**Figure 3C**). These results indicate that the therapeutic action of CPI-613 is significantly improved when administered together with a KD.

The KD elevates blood β-hydroxbutyrate levels while reducing blood glucose and the glucose/ ketone index (GKI) in young postnatal mice

Young mice (p25) were tested for the influence of KD on body weight, blood glucose and ketone levels, and the calculated GKI. Mice were fed the KD for 2 weeks when blood glucose and ketone were measured using the KetoMojo glucose/ketone meter. Following these measurements, the mice were implanted with VM-M3/luc (bioluminescent) cells as mentioned above. The diet was continued for another 2 weeks. The brains were removed and fixed in formalin for histology.

Blood glucose was 8-11 mM and 5-7 mM in the chow fed mice and the KD mice, respectively. This significant reduction of blood glucose in the KD-fed mice was associated with a significant elevation of blood ketone levels in KD fed mice i.e., 0.7 mM- 2.0 mM in chow group compared to 3.3 -3.9 mM in KD group mice. Accordingly, the GKI was significantly reduced in KD fed mice compared to that of chow fed mice. **(Figure 4A).**

These findings further suggest that KD therapy can reduce GKI values and tumor invasion compared to chow feeding alone. Histological analysis revealed that VM-M3 tumour cell invasion was markedly less in the brains of the mice fed the KD than in the mice fed the chow diet. Three independent mice brains were evaluated from each group **(Figure 4B).** These findings support the view that ketogenic metabolic therapy can be a potentially powerful therapy for children with malignant brain cancer.

Discussion

Our study is the first to report a robust therapeutic benefit of MBZ and CPI-613 for managing invasive glioma in a preclinical pediatric model of HGG. The data show a significant role of diet/drug therapy that targets glucose and glutamine simultaneously for managing the growth experimental pediatric glioma. We recently showed that the ketogenic diet, used together with the glutamine targeting drug DON, significantly increased the survival of adult VM/Dk mice when the VM-M3 tumor cells were implanted orthotopically into the brain (28). However, invasion of the VM-M3 cells from the cerebral cortex into the spinal cord was not observed in our previous studies using adult mice. In contrast to these findings, massive invasion into the spinal cord and

spinal meninges was seen when the VM-M3 cells were grown in the brain of p21 VM/Dk mice consistent with evidence that the most invasive cells in HGG are of mesenchymal origin like the VM-M3 cells (17, 18). Spinal cord invasion was not seen, however, in p21 mice that received cerebral implants of either the VM-NM or the CT-2A tumor cells that are of neural stem cell origin (17, 56). These findings support evidence that the microenvironment of the central nervous system in young mice is more conducive for spinal cord invasion of HGG cells of mesenchymal origin than is that of adult mice (10, 12). Hence, VM-M3 cells grown in the p21 mouse brain represents a good model for pediatric HGG.

We also showed for the first time that the antiparasitic drug, MBZ, could target the glutaminolysis pathway in VM-M3 glioma cells, which is linked to improving survival of the mice. Moreover, our findings showed that the PDH/α-KGDH inhibitor, CPI-613, was therapeutic against VM-M3 cell growth and invasion only when used together with the ketogenic diet. Ketogenic metabolic therapy, if administered appropriately in mice or humans, can be a powerful press therapy for reducing inflammation, proliferation, and angiogenesis while at the same time enhancing the death of malignant glioma cells (24, 57). Consequently, we administered MBZ and CPI-613 to the juvenile mice with the KD to improve bioavailability and reduce toxicity,

The p21 mice used in our study were administered the KD in daily amounts needed to maintain body weight, which can be challenging in young mice (58). All of the juvenile mice on KD achieved therapeutic ketosis within 3-4 days of diet treatment. The brain histology data showed that tumour growth was significantly less in the KD-fed mice than in the chow-fed mice. From our experience, the anti-cancer therapeutic effect of the KD is best when used against naturally arising tumors grown in their syngeneic host using fat:protein + carbohydrate ratios of 3:1 or 4:1. These ratios can also reduce the glucose ketone index (GKI) to 2.0 or below with modest to minimal body weight loss. Studies not adhering to these criteria often do not show anti-cancer effects of KD therapy (59-62). The therapeutic success of ketogenic metabolic therapy comes largely from optimizing the macronutrient and micronutrient composition of the KD in order to achieve the therapeutic GKI values (57, 63). As the basal metabolic rate is slower in humans than in mice, the therapeutic effects of the KD will be potentially more powerful in children with HGG than in mice with HGG. Glutamine-driven mesenchymal cells are the most invasive malignant

cells in HGG (23, 28). The KD will be less able to restrict growth of these neoplastic cells than those cells more dependent glucose. In this situation, the pulsing of glutamine targeting drugs can be used safely with ketogenic diet (the press) to maximize the therapeutic effect of drugs (57).

Previous studies showed that the bioavailability of MBZ was improved when administered with high fat meals (37, 39). Additional strategies used to increase drug bioavailability in tumors include alternative formulations of MBZ with vegetable oils, altering the crystalline structure, and PEGylation (64-67). Oral administration of MBZ (50 mg/kg mixed with sesame oil) in syngeneic and orthotopic glioma models in adult mice significantly extended mean survival up to 63% (30). We showed that the KD alone improved the survival of the tumor-bearing juvenile mice up to 100% over the chow-fed mice. Further improvement in survival was seen when we mixed the MBZ (100 mg/kg) in the KD. The cocktail of MBZ and DON with ketogenic diet extend the survival over 300%. We previously showed that DON is a powerful glutamine targeting drug that significantly inhibits VM-M3 tumor progression (28). Consequently, we included a DON-treated group as a positive control in our current study.

We previously showed that the KD could facilitate delivery of structurally different small molecules through the blood brain barrier (28, 68). DON delivery to the orthotopic VM-M3 tumor was three-fold greater when administered with a calorie restricted KD mice than when administered with standard high-carbohydrate mouse chow(28). Consequently, we did not include a chow MBZ mouse group in this study. Administration of MBZ and DON with the KD allowed for lower dosing thus eliminating issues of drug toxicity. Better overall mouse survival without observable toxicity was achieved when both MBZ and DON were administered with the KD. This information would be especially important when translating this therapeutic strategy to the clinic, as avoidance of any type of toxicity would be of upmost importance to children with HGG.

The therapeutic action of MBZ is due in part to inhibition of tubulin polymerization (30, 69). Tubulin polymerization is an ATP driven process in parasites (70). Previous reports have suggested that inhibition of carbohydrate metabolism might also account in part for the anti parasitic action of MBZ (71, 72). We now show that MBZ could block the glutamine utilization in VM-M3 cells *in-vitro* and could inhibit the expression of Glutaminase C in *in-vivo* tumor tissue.

Glutaminase C expression is directly related to the malignancy of different tumor cells and thus glutamine metabolism is elevated in many cancers (73-75). Metabolic cooperation of both glucose and glutamine is essential for the life cycle of both parasites and tumor cells (76). We described how glucose and glutamine are two major fuels that drive the cytoplasmic and mitochondrial substrate level phosphorylations necessary for tumor cell survival and growth (27). Further studies are needed to determine if MBZ could have therapeutic effects on other glutamine-dependent tumor cells.

A significant part of our study was the evaluation of CPI-613, commonly known as devimistat. CPI-613 targets the pyruvate dehydrogenase (PDH) and alpha-ketoglutarate dehydrogenase enzymes necessary for tumor growth and is in clinical trial for pancreatic cancer in combination with other drugs (44, 49). No prior studies, however, have evaluated the therapeutic action of CPI-613 against brain cancer. We found a significant dose-dependent effect of CPI-613 on VM-M3 cells *in-vitro.* These findings justified an evaluation of CPI-613 on the growth of VM-M3 in p21 mice. Remarkably, we showed that CPI-613 was effective in reducing VM-M3 tumor only when administered with the ketogenic diet. CPI-613 had no significant effect on VM-M3 tumor growth when administered a regular chow diet. In addition to improving survival of p21 VM/Dk mice bearing the VM-M3 tumor, the combination of ketogenic diet and CPI-613 also significantly improved overall survival in p21 C57BL/6 mice bearing the CT-2A neural stem cell tumor. Future experiments will investigate the level of CPI-613 in the tumor in the KD and chow fed brain as we did previously for DON (28). We hypothesize that the KD will also act as a vehicle for facilitating the delivery of CPI-613 through the blood brain barrier for HGG management.

The ketogenic diet, MBZ, and CPI-613 are presently in clinical trials for different types of cancers in adults and children. The ketogenic diet is already recognized as in the epilepsy clinic for children. MBZ is in clinical trial for pediatric recurrent/non-responsive brain tumors to check the safety and tolerability of doses. Our preclinical results in the juvenile in p21 will have a direct translational benefit to childhood brain cancer, if administered appropriately with KD. We also expect that this therapy could be effective for managing childhood HGG when used either alone or in combination with non-toxic aspects of standard of care. Additional preclinical studies are needed for CPI-613 in relevant brain tumor models before use in clinical trials for pediatric glioma.

Also, further investigations are underway in our laboratory using cocktails of MBZ, CPI-613, and DON and other anti-glutamine drugs with ketogenic diet for management of HGG. Our study will have a potential bench to bedside translation, especially for children with HGG.

Materials and Methods

Mice

Young mice (*p21-p25*) of the VM/Dk (VM) and C57BL/6J (B6) strain were used for this study. Studies were initiated one day after weaning. Males and females within and between litters were matched for age, sex and body weight. All mice used in this study were housed and bred in the Boston College Animal Care Facility using husbandry conditions as previously described (77). All animal procedures and protocols were in strict accordance with the NIH Guide for the Care and Use of Laboratory Animals and were approved by the Institutional Animal Care Committee at Boston College under assurance number A3905-01.

Pediatric syngeneic glioma model

The (p21-p25) mice were anaesthetized with isoflurane (5% in oxygen). The tops of the heads were shaved and disinfected with ethanol and a small incision was made in the scalp over the midline. A small indentation was made in the skull over the right parietal region behind the coronal suture and lateral to the sagittal suture using an 18G needle. VM-M3 tumour cells (approx. 100,000 in 5 ul PBS) were implanted in the right cerebral cortex approximately 1.5–2.0 mm deep using a Hamilton syringe. Betadine, a topical antiseptic, was applied before the skin flaps were closed with 7 mm reflex clips. The mice were placed in a warm room (24^{o} C) until they were fully recovered. The procedure confirms 100% recovery within a few hours of implantation. CT-2A tumour cells (approx. 100,000 in 5ul PBS) were implanted in C57/BL6 young mice (p21-p25) using the same procedure described above for VM-M3 cells.

Tumour cell lines

The VM-M3 tumour used in this study arose spontaneously in the cerebrum of an adult male mouse of the VM/Dk inbred strain. A cell line was prepared from the tumour as described previously. The VM-M3 tumour manifests all of the invasive characteristics seen in human GBM. The CT-

2A tumour was originally produced from implantation of 20-methylcholanthrene into the cerebral cortex of a C57BL/6J mouse and was broadly classified as a poorly differentiated highly malignant anaplastic astrocytoma and a cell line was produced from this tumour as described. More recent studies have classified the CT-2A tumour as a neural stem cell tumour. The VM-M3 and the CT-2A cell lines were transduced with a lentivirus vector containing the firefly luciferase gene under control of the cytomegalovirus promoter (VM-M3/Fluc, gift from Miguel Sena-Esteves, UMass Medical School). This transduction allows the cells to be tracked in the brain using bioluminescent imaging.

Dietary/Drug Regimens and Body Weight

All young mice received the standard chow diet for a day or two prior to initiation of the study. Tumour cells were implanted on day zero. Upon implantation of the tumour, mice remained on chow diet for 6 days until an *in-vivo* image was performed to confirm the tumor take for all mice. Mice were assigned to diet and drug groups on day 6. Male and female young mice were considered for each group. Mice receiving the standard chow diet (Lab Diet) *ad libitum* for the duration of the study. Ketogenic diet (KetoGEN, Medica Nutrition, Canada) were given *ad-libitum* so that the young mice can maintain the body weight for this short-term study.

Mebendazole (Sigma) was administered to the mice mix thoroughly in the KD (100 mg/kg body weight) for 3 days consecutively/wk. Mice food was monitored daily to approximate the equal amount of drug for each mouse. The KD, without MBZ, was administered alone on the off days. For those mice that received DON injections, a fresh stock (Sigma) was prepared and diluted to an appropriate concentration in PBS and was administered intraperitoneally (i.p.). The DON stock solution in PBS was stored at -20°C for the duration of the study and mice received 100-150 ul injections of 1.0 mg/kg. DON was injected once or twice a week depending on the overall health and tumor progression of the mice. Some doses were skipped if the mice appeared lethargic or if body weight loss exceeded 1.5 g from the previous day. Studies were terminated at the time of morbidity for the control groups.

CPI-613 (AdooQ Biosciences), was injected i.p. 0.5-1.0 mg/kg body weight once or twice in a week. CPI-613 stock is made in DMSO solution and fresh 100 times diluted solution was made in PBS before injection in mice. Similar dilution of DMSO was injected in the control group.

Bioluminescence Imaging

The Xenogen IVIS system is used to record the bioluminescent signal from the labeled tumours as we previously described. Briefly, for *in-vivo* imaging, mice received an i.p. injection of d-lucifierin (50 mg/kg) in PBS and Isoflurane (5% in oxygen). Imaging times ranged from 1 to 5 min, depending on the time point. For *ex-vivo* imaging, brains were removed and imaged in 0.3 mg d-luciferin in PBS. The IVIS Lumina cooled CCD camera system was used for light acquisition. Data acquisition and analysis was performed with Living Image software (Caliper LS).

Histology of brain and spinal cord

Brain tumour and spinal cord samples were fixed in 10% neutral buffered formalin (Sigma) and embedded in paraffin. Tissues were sectioned at 5 μm, were stained with haematoxylin and eosin (H&E) at the Harvard University Rodent Histopathology Core Facility (Boston, MA), and were examined by light microscopy using either a Zeiss Axioplan 2 or Nikon SMZ1500 light microscope. Images were acquired using SPOT Imaging Solutions (Diagnostic Instruments, Inc.) cameras and software. All histological sections were evaluated at the Harvard University Rodent Histopathology Core Facility.

Liquid Chromatography Mass Spectrometry Analysis of Metabolomics

VM-M3/luc cells were seeded ($1x10^5$) in 6 wells plate. After 24 hours the cells were treated with MBZ (1.0 uM) for 2, 6, and 12 hours in basal media with no FBS (25 mM glucose and 4.0 mM glutamine). After removing the media, 1.0 ml of ice cold methanol:water (80:1) mixture was added to each well and immediately transferred to -80ºC for 15 minutes. Plates were taken out at different time points and placed on ice, scraped, and the extract transferred to Eppendorf tubes. The tubes were vortexed and centrifuged at 10,000 x g for 10 minutes. The supernatant was transferred to a new tube and centrifuged at 30ºC. Cell extract was reconstituted in 100ul of methanol and then filtered through nylon before injecting into the LC/MS instrument (Agilent 6220 TOF, BPGbio global metabolomics platform).

Blood glucose and ketone measurements

All mice were fasted for 2 hours before blood collection to stabilize blood glucose levels. Blood glucose and ketone levels were measured using the Keto-Mojo monitoring system (keto-mojo, Napa, California). Whole blood from the tail was placed onto the glucose or ketone strip. The keto-mojo meter was used to determine the mmol levels of glucose and β-hydroxybutyrate in the blood. The Glucose Ketone Index (GKI) was determined as we previously described.

Western blot analysis of glutaminase protein expression.

Frozen tumour and normal brain tissues were homogenized in ice-cold lysis buffer containing 20 mmol/L Tris-HCl (pH 7.5), 150 mmol/L NaCl,1 mmol/L Na_2EDTA, 1 mmol/L EGTA, 1% Triton, 2.5 mmol/L NaPPi,1 mmol/L α-glycerophosphate, 1 mmol/L Na3PO4, 1 Ag/mL leupeptin, and 1 mmol/L phenylmethylsufonyl fluoride. Lysates were transferred to 1.7 mL Eppendorf tubes, mixed on a rocker for 1 h at 4°C, and then centrifuged at 8,100 x g for 20 min. Supernatants were collected and protein concentrations were estimated using the Bio-Rad detergent-compatible protein assay. Approximately 100 ug of total protein from each tissue sample was denatured with SDS-PAGE sample buffer [63 mmol/L Tris-HCl (pH 6.8), 10% glycerol, 2% SDS, 0.0025% bromphenol blue, and 5% 2-mercaptoethanol] and was resolved by SDS-PAGE on 4% to 12% Bis-Tris gels (Invitrogen). Proteins were transferred to a polyvinylidene difluoride immobilon TM-P membrane (Millipore) overnight at 4°C and blocked in either 5% nonfat powdered milk or 5% bovine serum albumin in TBS with Tween 20 (pH 7.6) for 1 to 3 h at room temperature. Membranes were probed with primary antibodies (glutaminase C, abcam, UK) overnight at 4°C with gentle shaking. The blots were then incubated with the appropriate secondary antibody (anti-rabbit) for 1 h at room temperature and bands were visualized with enhanced chemiluminescence. Each membrane was stripped and re-probed for β-actin as an internal loading control.

Statistics

Tumor bioluminescence *in-vitro*, *in-vivo*, and *ex-vivo* data were analyzed using the one-way analysis of variance (ANOVA) followed by Mann Whitney test or by a student's t test. In each figure, error bars are mean ± SEM and *n* is the number of individual mice analyzed. The Survival studies were plotted on a Kaplan-Meier curves were determined using Graph Pad Prizm software and significance was analyzed using the log-rank test.

Data availability

The authors declare that all data supporting the findings of this study are available upon request from the corresponding author. The source data for all figures are provided as a source data file.

Acknowledgements

We thank Children with Cancer UK (Grant Ref 19-313), Foundation for Metabolic Cancer Therapies, Dr. Edward Miller, Dr. Joseph Maroon, Andy Martin, the Corkin Family Foundation, Kenneth Rainin Foundation, the Delaware County Special Deputies Benevolent Fund, the Broken Science Initiative, and the Boston College Research Expense Fund for their support. We also thank Alexandra Chimento for helping with the animal work. We also thank Harvard Rodent core histopathology Lab and Dr. Rodereick Bronson for histological analysis.

Key words; spinal cord, glutaminolysis, glycolysis, metabolic therapy, press-pulse, glutamine, glycolysis, metastasis, invasion, glioblastoma.

Abbreviations: DMSO - dimethyl sulfoxide; PBS – phosphate bufferered saline; PDH – pyruvate dehydrogenase; α-KGDH – α - ketoglutarate dehydrogenase; OxPhos – oxidative phosphorylation; Na2EDTA - Disodium ethylenediaminetetraacetate dihydrate; Na3PO4 – trisodium phosphate; FBS – fetal bovine serum.

Reference:

1. Philips A, Henshaw DL, Lamburn G, O'Carroll MJ. Brain Tumours: Rise in Glioblastoma Multiforme Incidence in England 1995-2015 Suggests an Adverse Environmental or Lifestyle Factor. J Environ Public Health. 2018;2018:7910754.
2. Grech N, Dalli T, Mizzi S, Meilak L, Calleja N, Zrinzo A. Rising Incidence of Glioblastoma Multiforme in a Well-Defined Population. Cureus. 2020;12(5):e8195.
3. Bennett J, Erker C, Lafay-Cousin L, Ramaswamy V, Hukin J, Vanan MI, et al. Canadian Pediatric Neuro-Oncology Standards of Practice. Front Oncol. 2020;10:593192.
4. Siegel RL, Miller KD, Jemal A. Cancer statistics, 2016. CA Cancer J Clin. 2016;66(1):7-30.

5. Siegel RL, Miller KD, Wagle NS, Jemal A. Cancer statistics, 2023. CA Cancer J Clin. 2023;73(1):17-48.
6. Jung TY, Lee JY, Kim DS, Park HJ, Kim CY, Ra YS, et al. Pediatric supratentorial high-grade glioma: multicenter retrospective observational study of the Korean Society for Pediatric Neuro-Oncology. J Neurooncol. 2015;121(2):413-9.
7. Vanan MI, Eisenstat DD. Management of high-grade gliomas in the pediatric patient: Past, present, and future. Neurooncol Pract. 2014;1(4):145-57.
8. Kautiainen RJ, Na SD, King TZ. Neurological predictor scale is associated with academic achievement outcomes in long-term survivors of childhood brain tumors. J Neurooncol. 2019;142(1):193-201.
9. Li Z, Langhans SA. In Vivo and Ex Vivo Pediatric Brain Tumor Models: An Overview. Front Oncol. 2021;11:620831.
10. Wagner S, Benesch M, Berthold F, Gnekow AK, Rutkowski S, Strater R, et al. Secondary dissemination in children with high-grade malignant gliomas and diffuse intrinsic pontine gliomas. Br J Cancer. 2006;95(8):991-7.
11. Parsa AT, Wachhorst S, Lamborn KR, Prados MD, McDermott MW, Berger MS, et al. Prognostic significance of intracranial dissemination of glioblastoma multiforme in adults. J Neurosurg. 2005;102(4):622-8.
12. Vaidya SJ, Hargrave D, Saran F, Britton J, Soomal R, Bouffet E. Pattern of recurrence in paediatric malignant glioma: an institutional experience. J Neurooncol. 2007;83(3):279-84.
13. Morantz RA, Wood GW, Foster M, Clark M, Gollahon K. Macrophages in experimental and human brain tumors. Part 2: studies of the macrophage content of human brain tumors. J Neurosurg. 1979;50(3):305-11.
14. Caretti V, Sewing AC, Lagerweij T, Schellen P, Bugiani M, Jansen MH, et al. Human pontine glioma cells can induce murine tumors. Acta Neuropathol. 2014;127(6):897-909.
15. Wagner S, Czub S, Greif M, Vince GH, Suss N, Kerkau S, et al. Microglial/macrophage expression of interleukin 10 in human glioblastomas. Int J Cancer. 1999;82(1):12-6.
16. Huysentruyt LC, Akgoc Z, Seyfried TN. Hypothesis: are neoplastic macrophages/microglia present in glioblastoma multiforme? ASN neuro. 2011;3(4).
17. Huysentruyt LC, Mukherjee P, Banerjee D, Shelton LM, Seyfried TN. Metastatic cancer cells with macrophage properties: evidence from a new murine tumor model. Int J Cancer. 2008;123(1):73-84.
18. Shelton LM, Mukherjee P, Huysentruyt LC, Urits I, Rosenberg JA, Seyfried TN. A novel pre-clinical in vivo mouse model for malignant brain tumor growth and invasion. J Neurooncol. 2010;99(2):165-76.
19. Macartney G, Harrison MB, VanDenKerkhof E, Stacey D, McCarthy P. Quality of life and symptoms in pediatric brain tumor survivors: a systematic review. J Pediatr Oncol Nurs. 2014;31(2):65-77.
20. Gottardo NG, Gajjar A. Chemotherapy for malignant brain tumors of childhood. J Child Neurol. 2008;23(10):1149-59.
21. Cohen KJ, Heideman RL, Zhou T, Holmes EJ, Lavey RS, Bouffet E, et al. Temozolomide in the treatment of children with newly diagnosed diffuse intrinsic pontine gliomas: a report from the Children's Oncology Group. Neuro-oncology. 2011;13(4):410-6.
22. Vallejo FA, Shah SS, de Cordoba N, Walters WM, Prince J, Khatib Z, et al. The contribution of ketone bodies to glycolytic inhibition for the treatment of adult and pediatric glioblastoma. J Neurooncol. 2020;147(2):317-26.

23. Seyfried TN, Shelton L, Arismendi-Morillo G, Kalamian M, Elsakka A, Maroon J, et al. Provocative Question: Should Ketogenic Metabolic Therapy Become the Standard of Care for Glioblastoma? Neurochem Res. 2019;44(10):2392-404.
24. Seyfried TN, Arismendi-Morillo G, Zuccoli G, Lee DC, Duraj T, Elsakka AM, et al. Metabolic management of microenvironment acidity in glioblastoma. Front Oncol. 2022;12:968351.
25. Chinopoulos C, Seyfried TN. Mitochondrial Substrate-Level Phosphorylation as Energy Source for Glioblastoma: Review and Hypothesis. ASN neuro. 2018;10:1759091418818261.
26. Oizel K, Yang C, Renoult O, Gautier F, Do QN, Joalland N, et al. Glutamine uptake and utilization of human mesenchymal glioblastoma in orthotopic mouse model. Cancer & metabolism. 2020;8:9.
27. Seyfried TN, Arismendi-Morillo G, Mukherjee P, Chinopoulos C. On the Origin of ATP Synthesis in Cancer. iScience. 2020;23(11):101761.
28. Mukherjee P, Augur ZM, Li M, Hill C, Greenwood B, Domin MA, et al. Therapeutic benefit of combining calorie-restricted ketogenic diet and glutamine targeting in late-stage experimental glioblastoma. Commun Biol. 2019;2:200.
29. Bai RY, Staedtke V, Rudin CM, Bunz F, Riggins GJ. Effective treatment of diverse medulloblastoma models with mebendazole and its impact on tumor angiogenesis. Neuro Oncol. 2015;17(4):545-54.
30. Bai RY, Staedtke V, Aprhys CM, Gallia GL, Riggins GJ. Antiparasitic mebendazole shows survival benefit in 2 preclinical models of glioblastoma multiforme. Neuro Oncol. 2011;13(9):974-82.
31. Nygren P, Larsson R. Drug repositioning from bench to bedside: tumour remission by the antihelmintic drug mebendazole in refractory metastatic colon cancer. Acta Oncol. 2014;53(3):427-8.
32. Mudduluru G, Walther W, Kobelt D, Dahlmann M, Treese C, Assaraf YG, et al. Repositioning of drugs for intervention in tumor progression and metastasis: Old drugs for new targets. Drug Resist Updat. 2016;26:10-27.
33. Mukhopadhyay T, Sasaki J, Ramesh R, Roth JA. Mebendazole elicits a potent antitumor effect on human cancer cell lines both in vitro and in vivo. Clin Cancer Res. 2002;8(9):2963-9.
34. Kern P. Echinococcus granulosus infection: clinical presentation, medical treatment and outcome. Langenbecks Arch Surg. 2003;388(6):413-20.
35. Lacey E. Mode of action of benzimidazoles. Parasitol Today. 1990;6(4):112-5.
36. Canete R. Mebendazole Is a Potential Alternative in the Treatment of Giardia duodenalis Infection. Curr Ther Res Clin Exp. 2016;80:1-2.
37. Pantziarka P, Bouche G, Meheus L, Sukhatme V, Sukhatme VP, Vikas P. The Repurposing Drugs in Oncology (ReDO) Project. Ecancermedicalscience. 2014;8:442.
38. Partono F, Purnomo, Tangkilisan A. The use of mebendazole in the treatment of polyparasitism. Southeast Asian J Trop Med Public Health. 1974;5(2):258-64.
39. Guerini AE, Triggiani L, Maddalo M, Bonu ML, Frassine F, Baiguini A, et al. Mebendazole as a Candidate for Drug Repurposing in Oncology: An Extensive Review of Current Literature. Cancers (Basel). 2019;11(9).
40. Dawson M, Watson TR. The effect of dose form on the bioavailability of mebendazole in man. Br J Clin Pharmacol. 1985;19(1):87-90.

41. Stuart SD, Schauble A, Gupta S, Kennedy AD, Keppler BR, Bingham PM, et al. A strategically designed small molecule attacks alpha-ketoglutarate dehydrogenase in tumor cells through a redox process. Cancer & metabolism. 2014;2(1):4.
42. Alistar A, Morris BB, Desnoyer R, Klepin HD, Hosseinzadeh K, Clark C, et al. Safety and tolerability of the first-in-class agent CPI-613 in combination with modified FOLFIRINOX in patients with metastatic pancreatic cancer: a single-centre, open-label, dose-escalation, phase 1 trial. Lancet Oncol. 2017;18(6):770-8.
43. Bingham PM, Stuart SD, Zachar Z. Lipoic acid and lipoic acid analogs in cancer metabolism and chemotherapy. Expert Rev Clin Pharmacol. 2014;7(6):837-46.
44. Lee KC, Maturo C, Perera CN, Luddy J, Rodriguez R, Shorr R. Translational assessment of mitochondrial dysfunction of pancreatic cancer from in vitro gene microarray and animal efficacy studies, to early clinical studies, via the novel tumor-specific anti-mitochondrial agent, CPI-613. Ann Transl Med. 2014;2(9):91.
45. Reddy VB, Boteju L, Boteju A, Shen L, Kassahun K, Reddy N, et al. In Vitro and In Vivo Metabolism of a Novel Antimitochondrial Cancer Metabolism Agent, CPI-613, in Rat and Human. Drug Metab Dispos. 2022;50(4):361-73.
46. Zachar Z, Marecek J, Maturo C, Gupta S, Stuart SD, Howell K, et al. Non-redox-active lipoate derivates disrupt cancer cell mitochondrial metabolism and are potent anticancer agents in vivo. J Mol Med (Berl). 2011;89(11):1137-48.
47. Pardee TS, Anderson RG, Pladna KM, Isom S, Ghiraldeli LP, Miller LD, et al. A Phase I Study of CPI-613 in Combination with High-Dose Cytarabine and Mitoxantrone for Relapsed or Refractory Acute Myeloid Leukemia. Clin Cancer Res. 2018;24(9):2060-73.
48. Anderson R, Miller LD, Isom S, Chou JW, Pladna KM, Schramm NJ, et al. Phase II trial of cytarabine and mitoxantrone with devimistat in acute myeloid leukemia. Nat Commun. 2022;13(1):1673.
49. Philip PA, Buyse ME, Alistar AT, Rocha Lima CM, Luther S, Pardee TS, et al. A Phase III open-label trial to evaluate efficacy and safety of CPI-613 plus modified FOLFIRINOX (mFFX) versus FOLFIRINOX (FFX) in patients with metastatic adenocarcinoma of the pancreas. Future Oncol. 2019;15(28):3189-96.
50. Semple BD, Blomgren K, Gimlin K, Ferriero DM, Noble-Haeusslein LJ. Brain development in rodents and humans: Identifying benchmarks of maturation and vulnerability to injury across species. Prog Neurobiol. 2013;106-107:1-16.
51. Duma MN, Oszfolk NI, Boeckh-Behrens T, Oechsner M, Zimmer C, Meyer B, et al. Positive correlation between blood glucose and radiotherapy doses to the central gustatory system in Glioblastoma Multiforme patients. Radiat Oncol. 2019;14(1):97.
52. Pitter KL, Tamagno I, Alikhanyan K, Hosni-Ahmed A, Pattwell SS, Donnola S, et al. Corticosteroids compromise survival in glioblastoma. Brain. 2016;139(Pt 5):1458-71.
53. Lemberg KM, Vornov JJ, Rais R, Slusher BS. We're Not "DON" Yet: Optimal Dosing and Prodrug Delivery of 6-Diazo-5-oxo-L-norleucine. Mol Cancer Ther. 2018;17(9):1824-32.
54. Shelton LM, Huysentruyt LC, Seyfried TN. Glutamine targeting inhibits systemic metastasis in the VM-M3 murine tumor model. Inter J Cancer 2010;127(10):2478-85.
55. Flores RE, Brown AK, Taus L, Khoury J, Glover F, Kami K, et al. Mycoplasma infection and hypoxia initiate succinate accumulation and release in the VM-M3 cancer cells. Biochimica et biophysica acta. 2018.

56. Binello E, Qadeer ZA, Kothari HP, Emdad L, Germano IM. Stemness of the CT-2A Immunocompetent Mouse Brain Tumor Model: Characterization In Vitro. Journal of Cancer. 2012;3:166-74.
57. Seyfried TN, Yu G, Maroon JC, D'Agostino DP. Press-pulse: a novel therapeutic strategy for the metabolic management of cancer. Nutr Metab (Lond). 2017;14:19.
58. Greene AE, Todorova MT, McGowan R, Seyfried TN. Caloric restriction inhibits seizure susceptibility in epileptic EL mice by reducing blood glucose. Epilepsia. 2001;42(11):1371-8.
59. Xia S, Lin R, Jin L, Zhao L, Kang HB, Pan Y, et al. Prevention of Dietary-Fat-Fueled Ketogenesis Attenuates BRAF V600E Tumor Growth. Cell Metab. 2017;25(2):358-73.
60. Liskiewicz AD, Kasprowska D, Wojakowska A, Polanski K, Lewin-Kowalik J, Kotulska K, et al. Long-term High Fat Ketogenic Diet Promotes Renal Tumor Growth in a Rat Model of Tuberous Sclerosis. Sci Rep. 2016;6:21807.
61. Dang MT, Wehrli S, Dang CV, Curran T. The Ketogenic Diet Does Not Affect Growth of Hedgehog Pathway Medulloblastoma in Mice. PloS one. 2015;10(7):e0133633.
62. De Feyter HM, Behar KL, Rao JU, Madden-Hennessey K, Ip KL, Hyder F, et al. A ketogenic diet increases transport and oxidation of ketone bodies in RG2 and 9L gliomas without affecting tumor growth. Neuro Oncol. 2016;18(8):1079-87.
63. Meidenbauer JJ, Mukherjee P, Seyfried TN. The glucose ketone index calculator: a simple tool to monitor therapeutic efficacy for metabolic management of brain cancer. Nutr Metab (Lond). 2015;12:12.
64. Ali DN, Chick BF. The effect of an oil formulation on the systemic availability of oxfendazole. Int J Parasitol. 1992;22(4):541-3.
65. Chiba Y, Kohri N, Iseki K, Miyazaki K. Improvement of dissolution and bioavailability for mebendazole, an agent for human echinococcosis, by preparing solid dispersion with polyethylene glycol. Chem Pharm Bull (Tokyo). 1991;39(8):2158-60.
66. Garcia-Rodriguez JJ, de la Torre-Iglesias PM, Vegas-Sanchez MC, Torrado-Duran S, Bolas-Fernandez F, Torrado-Santiago S. Changed crystallinity of mebendazole solid dispersion: improved anthelmintic activity. Int J Pharm. 2011;403(1-2):23-8.
67. Liu CS, Zhang HB, Jiang B, Yao JM, Tao Y, Xue J, et al. Enhanced bioavailability and cysticidal effect of three mebendazole-oil preparations in mice infected with secondary cysts of Echinococcus granulosus. Parasitol Res. 2012;111(3):1205-11.
68. Denny CA, Heinecke KA, Kim YP, Baek RC, Loh KS, Butters TD, et al. Restricted ketogenic diet enhances the therapeutic action of N-butyldeoxynojirimycin towards brain GM2 accumulation in adult Sandhoff disease mice. Journal of neurochemistry. 2010;113(6):1525-35.
69. Doudican N, Rodriguez A, Osman I, Orlow SJ. Mebendazole induces apoptosis via Bcl-2 inactivation in chemoresistant melanoma cells. Mol Cancer Res. 2008;6(8):1308-15.
70. McNally FJ, Roll-Mecak A. Microtubule-severing enzymes: From cellular functions to molecular mechanism. J Cell Biol. 2018;217(12):4057-69.
71. Dogra N, Kumar A, Mukhopadhyay T. Fenbendazole acts as a moderate microtubule destabilizing agent and causes cancer cell death by modulating multiple cellular pathways. Sci Rep. 2018;8(1):11926.
72. Ahmad M, Nizami WA. In vitro effects of mebendazole on the carbohydrate metabolism of Avitellina lahorea (Cestoda). J Helminthol. 1987;61(3):247-52.
73. Knox WE, Linder M, Friedell GH. A series of transplantable rat mammary tumors with graded differentiation, growth rate, and glutaminase content. Cancer research. 1970;30(2):283-7.

74. Myint ZW, Sun RC, Hensley PJ, James AC, Wang P, Strup SE, et al. Evaluation of Glutaminase Expression in Prostate Adenocarcinoma and Correlation with Clinicopathologic Parameters. Cancers (Basel). 2021;13(9).
75. Katt WP, Cerione RA. Glutaminase regulation in cancer cells: a druggable chain of events. Drug Discov Today. 2014;19(4):450-7.
76. Nitzsche R, Zagoriy V, Lucius R, Gupta N. Metabolic Cooperation of Glucose and Glutamine Is Essential for the Lytic Cycle of Obligate Intracellular Parasite Toxoplasma gondii. J Biol Chem. 2016;291(1):126-41.
77. Flavin HJ, Wieraszko A, Seyfried TN. Enhanced aspartate release from hippocampal slices of epileptic (El) mice. J Neurochem. 1991;56(3):1007-11.

Figure 1 A

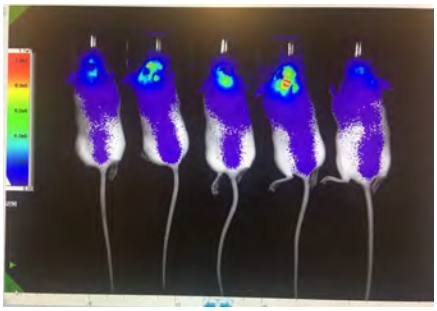

Figure 1 B

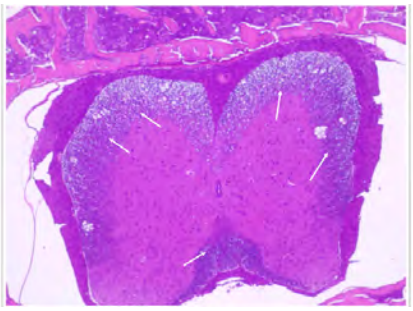

Figure 1 C

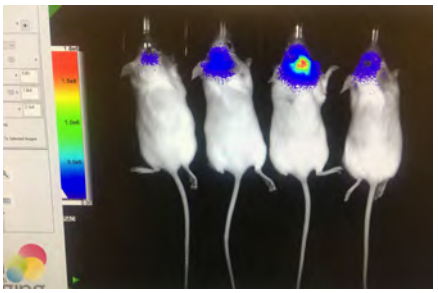

Figure 1 D

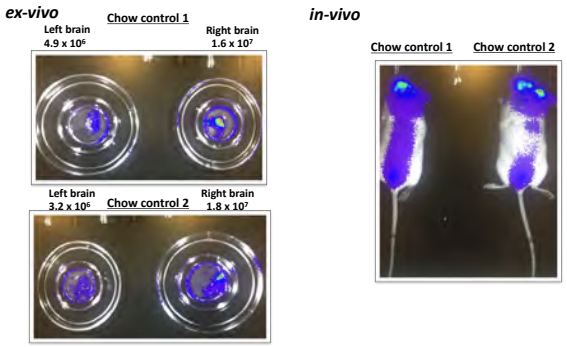

Figure 1 E

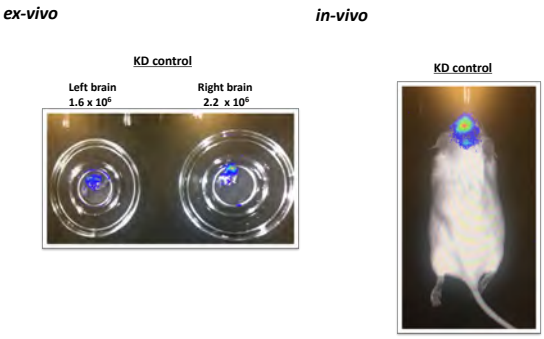

Figure1 F

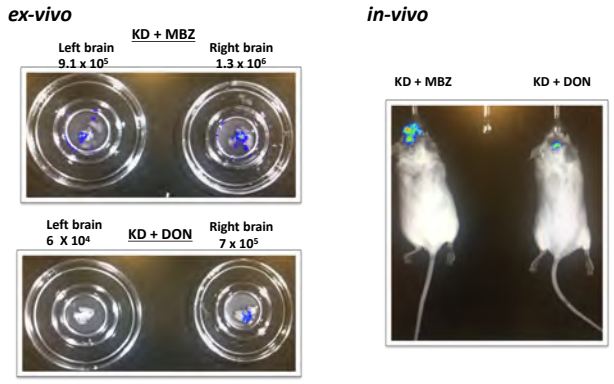

Figure 1 G

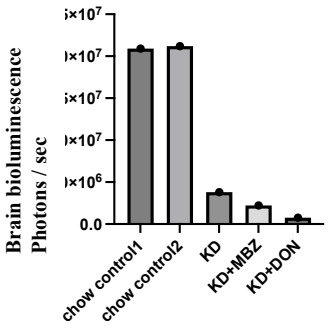

Figure1 H

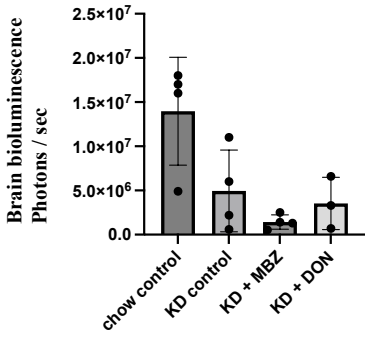

Figure1 I

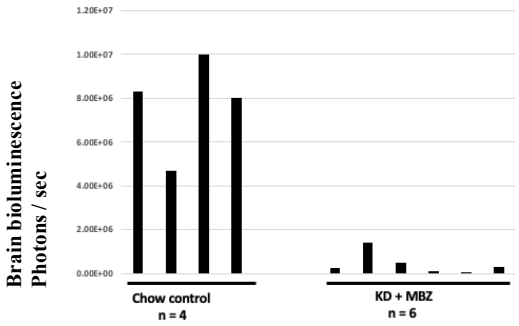

Figure1 J

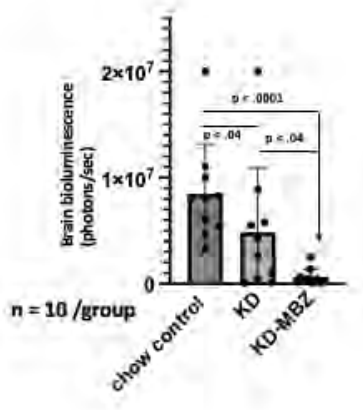

Figure1 K

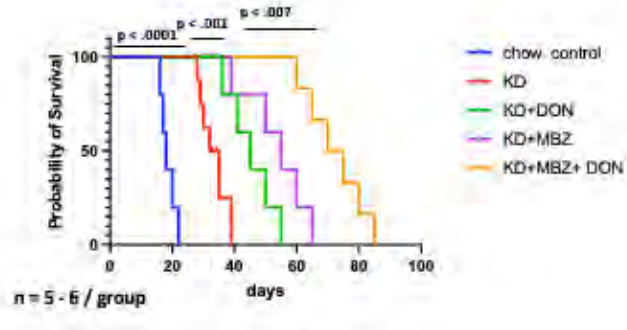

Figure1 L

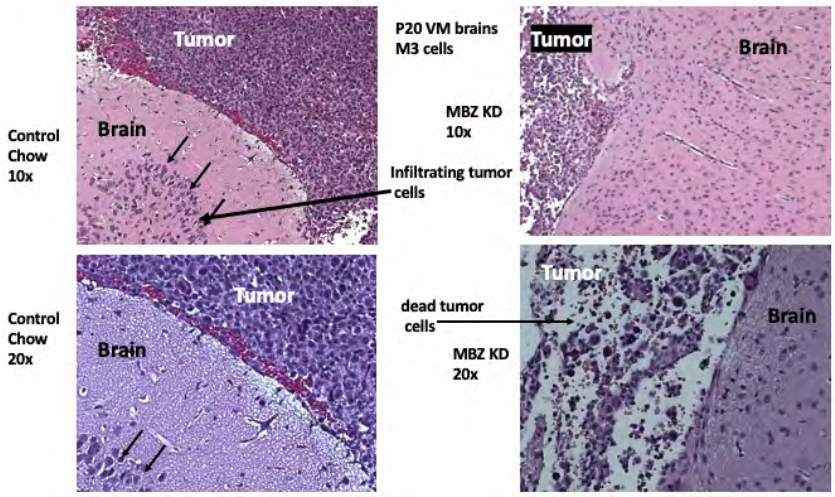

Figure 1. Effects of MBZ used with KD on orthotopically implanted VM-M3 glioblastoma cells in the brain of p20-25 VM/Dk mice. **A.** VM-M3 tumour cells invasion from the brain implantation site to the spinal column. This finding is indicative of tumour cell spread through CSF (*in vivo* analysis). **B.** Histological analysis of tumor cell invasion in the spinal cord. Dense infiltrates of tumor cells all around the spinal cord includes meninges. **C.** VM-NM glioma non-invasive stem cell tumour into young mice brain. Spinal cord invasion was not seen following brain implantation. **D.** *ex-vivo* and *in-vivo* bioluminescence image and photon counts of the brains of mice receiving the control standard mouse chow diet. The "right" ipsilateral side of the brain (tumour implanted side) showed significant bioluminescence. Bioluminescence detected on the "left" contralateral side is indicative of significant distal hemispheric invasion of the tumour cells (*ex-vivo* analysis). **E.** *ex-vivo* and *in-vivo* bioluminescence image and photon counts of the brains of mice receiving the Ketogenic diet (KD). No apparent spread of VM-M3 to the spinal column was detected on *in-vivo* analysis. Bioluminescence in the ipsilateral and contralateral brain was noticeably lower in the KD-fed mice than in the Chow-fed control mice. **F.** *ex-vivo* and *in-vivo* bioluminescence image and photon counts of the brains of mice receiving either KD + MBZ or KD + DON. Brain bioluminescence was noticeably lower in these two groups than in either the Chow control or the KD alone groups. Remarkably, no bioluminescent tumour cells were detected on the "left" contralateral brain side of the mouse treated in the KD + DON mice indicating that this treatment significantly reduced growth and distal invasion of the VM-M3 tumour cells. **G**. *ex-vivo* bioluminescence values from the five mice mentioned above. **H-I-J.** Experiment 2 and 3, further evaluation of the influence of diet and drugs on *ex-vivo* bioluminescence. Values are expressed as the mean ± SEM and Mann-Whitney test to determine the significance between the groups. **K.** The data from Experiment 4 showed that overall survival was longer in the KD-fed mice than in the chow-fed control mice, but that the overall survival was significantly longer in mice receiving the KD containing either MBZ or DON than in mice receiving the KD alone. Log-rank (Mantel-Cox test) analysis was performed to determine the significance between groups. **L.** The juvenile (p20) mice were implanted with VM-M3 tumour cells into the cerebral cortex and brain tissue histology (H&E) evaluated 12 days later. The low power (10x) and higher power (20x) images on the left show many VM-M3 cells invading into normal appearing brain tissue in a mouse fed the chow control diet. Massive tumour cell death without obvious invasion is shown in the low power (10x) and higher power (20x) images on the right in a mouse fed the KD + MBZ diet. These findings further suggest that administration of MBZ with a KD could offer a powerful non-toxic therapy for children with malignant brain cancer.

Figure2 A

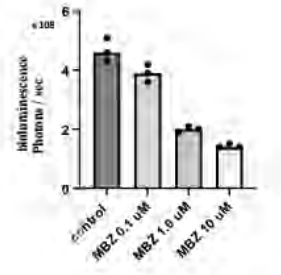

Figure2 B

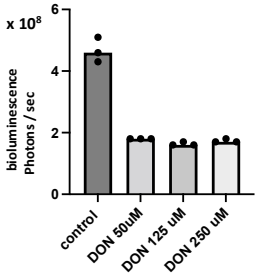

Figure2 C

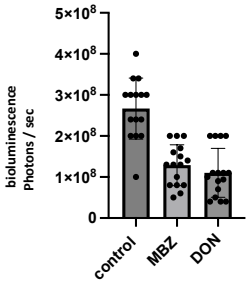

Figure 2 D

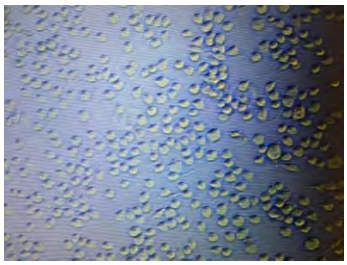

Figure2 E

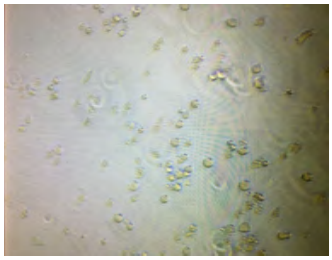

Figure 2 F

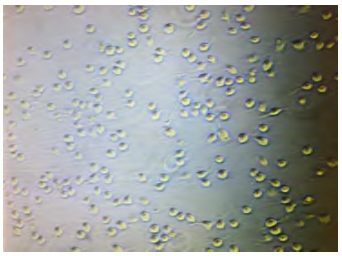

Figure 2 G

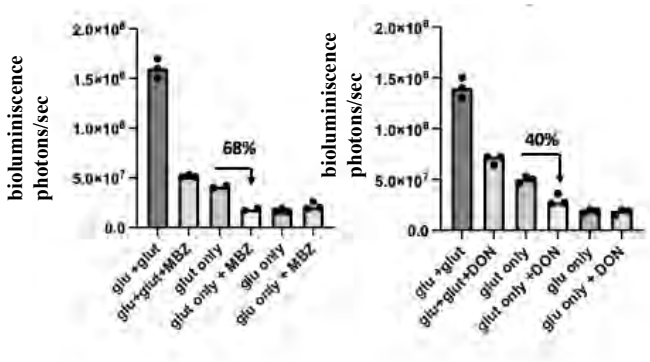

Figure2 H

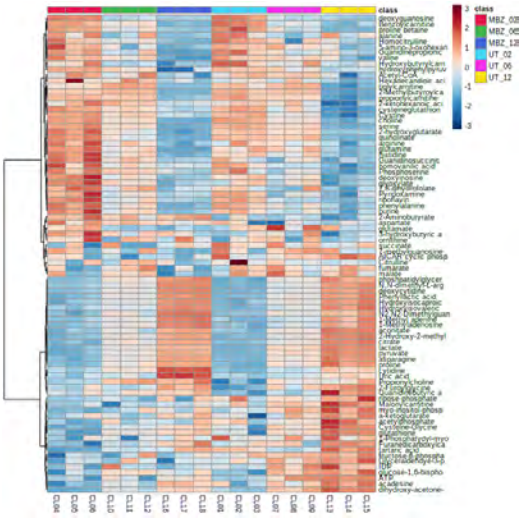

Figure2 I

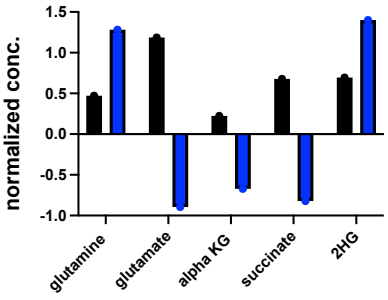

Figure2 J

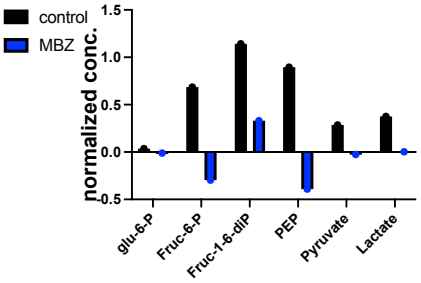

Figure2 K

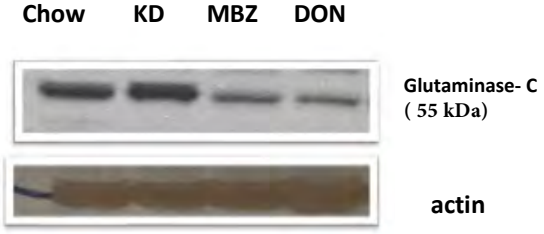

Figure 2. Evidence showing that MBZ targets both glutaminolysis and the glycolysis pathways in cultured VM-M3 cells. VM-M3 cells were treated with different doses of MBZ and DON while grown *in-vitro*. DON was used as a positive control. MBZ reduced the bioluminescence in the VM-M3 cells in a dose dependent manner **(A, C).** Brightfield images showed that MBZ killed the VM-M3 cells at the highest dose **(E)**. DON reduced the proliferation rate of VM-M3 cells but did not kill the cells (**B, F**). Experiments were repeated three times and values are expressed as the mean ± SEM and Mann-Whitney test to determine the significance between the groups. VM-M3 cells are more glutamine dependent than glucose for proliferation and MBZ kill the cells when glutamine is the only substrate in the media. (**G**). The LCMS metabolite data showed that MBZ reduced the glutaminolysis and glycolysis pathway (**H-J**). Mice brains were analyzed for glutaminase C expression. A significant reduction in glutaminase C expression in MBZ treated brain than in control groups. DON was used as a positive control (**K**).

Figure 3

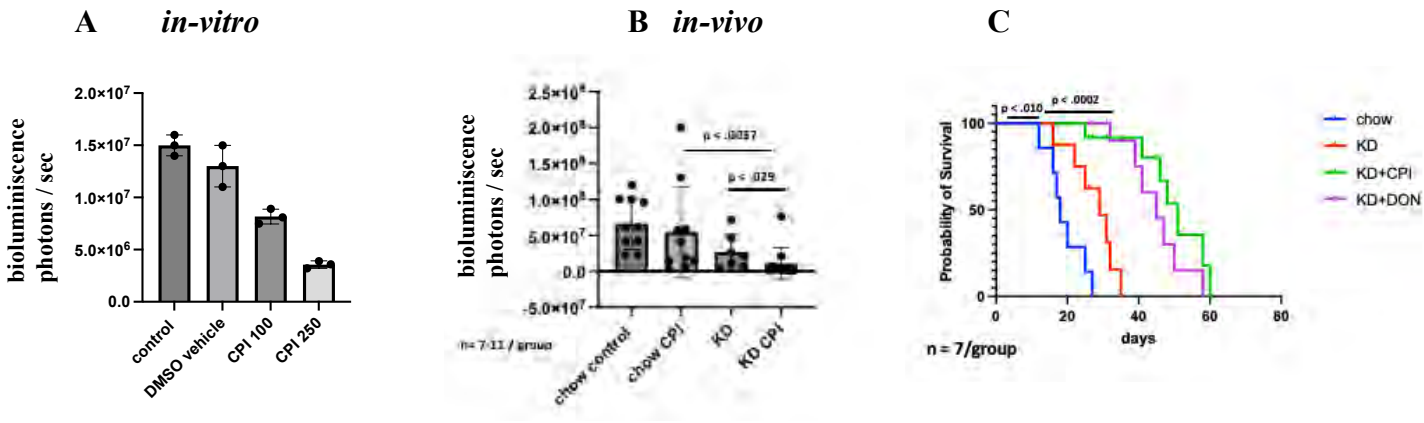

Figure 4

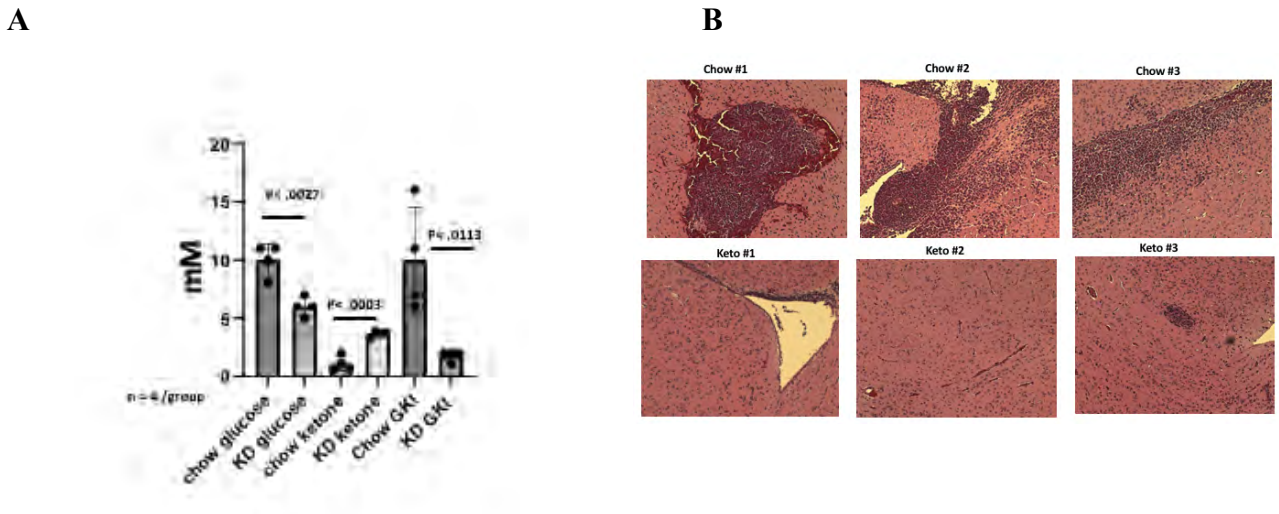

Figure 3. Effects of CPI-613 (devimistat) in the progression of VM-M3 cells grown *in-vitro* and *in -vivo* and survival of young mice with orthotopic CT-2A tumour.

VM-M3 cells were treated with different doses of CPI-613 while grown *in-vitro*. CPI-613 reduced the bioluminescence in the VM-M3 cells in a dose dependent manner **(A).** brain bioluminescence was least in KD + CPI group **(B).** Values are expressed as the mean ± SEM and Mann-Whitney test to determine the significance between the groups. Overall survival was significantly longer in CPI-613 treated young mice with CT-2A tumor in the brains compared to control groups **(C).** DON was used as a positive control. Log-rank (Mantel-Cox test) analysis was performed to determine the significance between groups.

Figure 4. Influence of the KD on blood glucose, β-hydroxybutarate, and the glucose ketone index (GKI) values in p20-25mice on ketogenic diet and histology of the brains with VM-M3 cells.

Young mice (p25) were tested for the ketogenic diet tolerability and blood glucose and ketone level in their blood. VM-M3 cells were implanted in the brains as described in Figure 1. A significant reduction of blood glucose is associated with a significant elevation of blood ketone levels in KD fed mice and accordingly GKI **(A)**. Values are expressed as the mean ± SEM and unpaired t test determines the significance between the groups. Brain tissue histology was evaluated 14 days after tumor implantation. The low power (10x) images on the top show many VM-M3 cells invading into normal appearing brain tissue in a chow-fed control mice. Images on the bottom show a reduction of tumor cells with less invasion in KD-fed mice. 3 independent mice brains were fixed, processed and imaged **(B).**